Journal of Power Sources 195 (2010) 5610–5618

Contents lists available at ScienceDirect

Journal of Power Sources

journal homepage: www.elsevier.com/locate/jpowsour

Pre-oxidized and nitrided stainless steel alloy foil for proton exchange membrane fuel cell bipolar plates: Part 1. Corrosion, interfacial contact resistance, and surface structure

M.P. Brady[a,*], H. Wang[b], J.A. Turner[b], H.M. Meyer III[a], K.L. More[a], P.F. Tortorelli[a], B.D. McCarthy[a]

[a] Oak Ridge National Laboratory, Oak Ridge, TN 37831-6115, USA
[b] National Renewable Energy Laboratory, Golden, CO 80401, USA

ARTICLE INFO

Article history:
Received 29 January 2010
Received in revised form 12 March 2010
Accepted 15 March 2010
Available online 20 March 2010

Keywords:
Polymer electrolyte/proton exchange membrane (PEM) fuel cells
Nitride
Metallic bipolar plates
Durability
Corrosion resistance

ABSTRACT

Thermal (gas) nitridation of stainless steel alloys can yield low interfacial contact resistance (ICR), electrically conductive and corrosion-resistant nitride containing surface layers (Cr_2N, CrN, TiN, V_2N, VN, etc.) of interest for fuel cells, batteries, and sensors. This paper presents results of scale-up studies to determine the feasibility of extending the nitridation approach to thin 0.1 mm stainless steel alloy foils for proton exchange membrane fuel cell (PEMFC) bipolar plates. Developmental Fe–20Cr–4V alloy and type 2205 stainless steel foils were treated by pre-oxidation and nitridation to form low-ICR, corrosion-resistant surfaces. As-treated Fe–20Cr–4V foil exhibited target (low) ICR values, whereas 2205 foil suffered from run-to-run variation in ICR values, ranging up to 2× the target value. Pre-oxidized and nitrided surface structure examination revealed surface-through-layer-thickness V-nitride particles for the treated Fe–20Cr–4V, but near continuous chromia for treated 2205 stainless steel, which was linked to the variation in ICR values. Promising corrosion resistance was observed under simulated aggressive PEMFC anode- and cathode-side bipolar plate conditions for both materials, although ICR values were observed to increase. The implications of these findings for stamped bipolar plate foils are discussed.

1. Introduction

Thin (~0.1 mm) stamped stainless steel alloy foils for proton exchange membrane fuel cell (PEMFC) bipolar plates offer the potential for significantly lower cost than currently used machined graphite bipolar plates, and reduced stack volume and better amenability to rapid, high-volume manufacturing than developmental polymer/carbon fiber and graphite composite bipolar plates [1–9]. The key challenges for stainless steels as bipolar plates are corrosion resistance and interfacial contact resistance (ICR) [1–13]. Stainless steels tend to exhibit borderline corrosion resistance in PEMFC bipolar plate environments, which can result in metal ion dissolution and possible poisoning and performance degradation of the PEMFC membrane [14], although recent work suggests that membrane proton conductivity may be more tolerant of metal ion contamination than the 5–10 parts per million (ppm) levels some earlier work suggested [15]. The primary drawback for stainless steels as bipolar plates is their high ICR values (despite high bulk electrical conductivity), which results from the passive oxide surface layer that confers corrosion resistance to stainless steels [1–10]. Typical ICR values for stainless steels [11] at the compaction forces of interest for PEMFC bipolar plates, ~150–200 N cm^{-2}, are at least an order of magnitude higher than the United States Department of Energy (USDOE) target of 10 mΩ cm^2 (discussed in Ref. [9]). This leads to high electrical resistance and unacceptable fuel cell stack performance.

Some metal nitrides are highly corrosion resistant and offer electrical conductivities up to an order of magnitude larger than that of graphite [16]. Proof-of principle evaluation of nitrided model Ni–Cr base alloys [9,17–19] indicated that thermally grown Cr-nitride surfaces exhibited excellent corrosion resistance and maintained low ICR values in PEMFC environments. A key advantage of the thermal nitridation approach is that it can potentially yield pin-hole defect free surface layers due to the high processing temperatures (~800–1100 °C) favoring reaction of all exposed metal surfaces [9,17–22]. Other groups have also recently reported promising results for thermally grown nitrides and/or nitride based deposited coatings to protect PEMFC bipolar plates [23–39].

The primary drawback of the thermal nitridation approach is that it only yields protective surfaces for a narrow range of alloy compositions and processing conditions [9]. Unfortunately, the Ni–(30–50) Cr weight percent (wt.%) base alloys that have proven amenable to this approach are too expensive for automotive

* Corresponding author at: ORNL, Materials Science and Technology, MS 6115, Oak Ridge, TN 37831-6115, USA. Tel.: +1 865 574 5153; fax: +1 865 241 0215.
E-mail address: bradymp@ornl.gov (M.P. Brady).

0378-7753/$ – see front matter © 2010 Elsevier B.V. All rights reserved.
doi:10.1016/j.jpowsour.2010.03.055

Table 1
Alloy compositions as determined by inductively coupled plasma and combustion analysis.

Fe–20Cr–4V Sheet	Fe–20Cr–3.88V–0.01Si–0.0081N–0.001C
Fe–20Cr–4V Foil	Fe–19.97Cr–3.82V–0.07Mn–0.07Si–0.0592N–0.03Ca–0.018C–0.01Al
2205 Foil	Fe–22.05Cr–5.64Ni–3.18Mo–0.49Mn–0.4Si–0.25Cu–0.2V–0.1Co–0.06W–0.03Nb–0.187N–0.023C

applications, although they may be economically viable for some stationary or portable power applications. Iron-base stainless steel alloys can potentially meet the USDOE automotive bipolar plate cost targets (equates roughly to ~$1–2/plate depending on stack performance). However, stainless steels exhibit high permeability to nitrogen, which results in very poor corrosion resistance due to extensive internal Cr-nitride precipitation in the alloy on nitridation instead of the desired continuous, protective Cr-nitride surface layer observed on nitrided Ni–(30–50)Cr base alloys [9,22].

This limitation for nitridation of Fe-base stainless steels can be bypassed under select conditions if oxygen is also present in the nitriding environment [9,19,21,22]. Two effects were observed: (1) the formation of a nitrogen-modified passive oxide surface layer (NMPOL) on high-Cr superferritic alloys (~27–29 wt.% Cr), such as 446 MOD-1 or AL29-4C®, which was composed of a complex, heterogeneous surface mixture of Cr-nitrides, Cr and Al oxides, and Ti-nitride [19,21]; and (2) the formation of a continuous Cr(V)-nitride surface layer overlaying an intermixed Cr(V)-oxide and -nitride underlayer which was observed for a developmental Fe–27Cr–6V wt.% bipolar plate alloy [9,22]. (The addition of V was found to be beneficial in promoting conversion of the thermally grown oxide to nitride on nitridation [22].) Excellent corrosion resistance and low ICR values were observed in simulated PEMFC bipolar plate environments for both types of surfaces.

Two significant challenges exist for transferring either approach to high volume bipolar plate production. First, the surface layers were formed in sealed nitriding environments, such that the oxygen was gettered during the course of the reaction and the environment gradually changed from oxidizing to nitriding. Although possible in a small laboratory-scale furnace, it is unlikely to be sufficiently controllable in large-scale production. Second, these higher-Cr alloys were susceptible to the formation of brittle sigma phase during heating and cooling to/from the 900–1100 °C nitridation temperature, which resulted in embrittled bipolar plates that fractured under load.

A potential solution to controllably forming surface nitride/oxide mixtures is to perform a short pre-oxidation step prior to nitridation. Preliminary attempts for Fe–27Cr–6V yielded the desired intermixed nitride/oxide surface structure [9,22]. Promising corrosion resistance and ICR values results were also recently reported for controlled pre-oxidation and nitridation of type 446 stainless steels [40]. To reduce the risk of sigma phase formation, and improve formability for stamping, lower Cr levels than the high-Cr superferritics studied to date are of interest. Part 1 of this paper presents the results of efforts to form corrosion-resistant, low-ICR nitride-oxide surfaces on stainless steel alloy foils in a manner amenable to commercial scale production. Part 2 [41] will present the results of single-cell fuel cell studies using stamped and pre-oxidized/nitrided stainless steel foils with performance benchmarked relative to untreated stainless steel foils and graphite bipolar plates.

2. Experimental

Exploratory studies of pre-oxidation and nitridation of a series of ferritic, duplex, and austenitic Fe–(18–27Cr)–(2–6)V–(0–10Ni) alloys were conducted using coupons obtained from small laboratory-scale arc-castings (~100–500 g) [42]. Preliminary evaluation suggested that the best combination of low ICR and high corrosion resistance on nitriding was exhibited by a ferritic Fe–20Cr–4V wt.% alloy, which is the subject of the present work. This Cr level was optimized to be low enough to achieve sufficient alloy ductility to permit foil manufacture/stamping and to minimize the potential for brittle sigma phase formation, but high enough in combination with V to yield low ICR, corrosion-resistant nitride surfaces.

In the present work, Fe–20Cr–4V was studied in two product forms: (1) 20 mm × 10 mm × 1 mm sheet coupons obtained from a ~500 g laboratory arc casting that was hot rolled to a 40% reduction at 900 °C and annealed at 900 °C for 10 min, and (2) a trial batch of 0.1 mm thick Fe–20Cr–4V foil processed using conventional commercial ferritic alloy hot/cold rolling and annealing conditions (details proprietary). The laboratory sheet coupons were polished to a #240 grit surface finish using SiC paper. The trial-scale foil production annealing equipment available for this work did not have sufficient hydrogen dew point control to prevent foil oxidation during annealing. This resulted in foil with a thin oxide layer (heat treatment "tint"), which was readily removed by light scrubbing with a "non-scratch" (polymer fiber) kitchen scouring pad. The chemistry of Fe–20Cr–4V bulk coupon and foil are shown in Table 1. For comparative purposes, 0.1 mm thick commercial foil of duplex 2205 stainless steel was also studied (Table 1). This alloy was selected due to its comparable Cr level (22% Cr) to Fe–20Cr–4V and its reported excellent corrosion resistance in PEMFC environments (data from commercial sheet material [11]).

Pre-oxidation and nitridation steps were conducted in separate furnace runs to gain insight into surface chemistry changes that resulted from each step. Pre-oxidation was conducted in flowing N_2–$4H_2$–$0.5O_2$ (volume percent), which was selected to produce a low oxygen partial pressure environment sufficient to oxidize controllably while potentially minimizing migration of Fe to the oxide surface due to the relatively low thermodynamic stability of Fe-oxides. Nitridation was conducted in ultrahigh purity N_2–$4H_2$ passed through a commercial molecular sieve to getter oxygen and moisture impurities. A wide range of pre-oxidation and nitridation conditions and furnace protocols were evaluated. Typical protocol initially involved loading samples into a horizontal quartz tube furnace, evacuation at room temperature to a 10^{-6} to 10^{-7} Torr vacuum, introduction of flowing N_2–$4H_2$–$0.5O_2$ or scrubbed N_2–$4H_2$ gas for 2 h at room temperature, 4 h heating to the reaction temperature (typically 900–1000 °C), holding at the reaction temperature and overnight furnace cooling to room temperature.

Some run-to-run scatter in the degree of O/N mass uptake was observed on nitridation, primarily as a result of varying levels of oxygen impurities in the furnace likely due to adsorption of moisture on the inner furnace surfaces during sample loading. In the latter stages of this work, this issue was solved by performing a 200–400 °C overnight vacuum bake out of the furnace after loading with test samples, prior to introducing the pre-oxidation or nitridation gases. This bake-out step was needed because of the relatively low thermodynamic stability of Cr with nitrogen as compared with oxygen. For example, only ~10 ppm oxygen is needed in N_2–$4H_2$ to favor Cr_2O_3 formation over CrN at 900 °C [9,22]. It should be noted that the 12 h overnight timeframe for this bakeout was selected for convenience, and that much shorter bakeout times are feasible.

Pre-oxidized and nitrided samples were characterized using techniques selected among X-ray diffraction (XRD) using Cu K_α radiation, Auger electron spectroscopy (AES), field emission gun

Table 2
Pre-oxidation and nitridation processing summary.

Alloy	Pre-oxidation (mass gain mg cm^{-2})	Nitridation (mass gain mg cm^{-2})	Bakeout	Figure
Fe–20Cr–4V sheet	925 °C/2 h: 0.23	900 °C/24 h: 0.18	–	Figs. 1 and 2
Fe–20Cr–4V sheet	925 °C/2 h: 0.22	1000 °C/1 h: 0.06	–	Figs. 1 and 2
Fe–20Cr–4V sheet	925 °C/2 h: 0.077	1000 °C/4 h: 0.38	–	Fig. 8
Fe–20Cr–4V sheet	900 °C/2 h: 0.18	–	–	Fig. 9b
Fe–20Cr–4V sheet	900 °C/2 h: 0.17	1000 °C/2 h: 0.12	–	Fig. 9c
Fe–20Cr–4V foil	900 °C/2 h: 0.08	1000 °C/2 h: 0.13	–	Figs. 3 and 4 anode
Fe–20Cr–4V foil	900 °C/2 h: 0.09	1000 °C/2 h: 0.11	–	Figs. 3 and 4 cathode
Fe–20Cr–4V foil	900 °C/1 h: 0.04	–	–	Fig. 10b
Fe–20Cr–4V foil	900 °C/1 h: 0.05	1000 °C/2 h: 0.15	1	Fig. 10c
2205 foil	900 °C/2 h: 0.06	1000 °C/2 h: 0.16	–	Fig. 4 high ICR
2205 foil	900 °C/2 h: 0.07	1000 °C/2 h: 0.18	1	Figs. 3 and 4 anode
2205 foil	900 °C/30 min: 0.08	1000 °C/2 h: 0.14	–	Figs. 3–5 cathode
2205 foil	900 °C/15 min: 0.06	1000 °C/4 h: 0.14	2	Fig. 7
2205 foil	900 °C/2 h: 0.07	1000/2: 0.158	2	Fig. 6a
2205 foil	900 °C/1 h 0.10	1000 °C/2 h: 0.005	1	Fig. 6b

1: 200 °C/12 h vacuum bake out. 2: 400 °C/12 h vacuum bake out.

(FEG) scanning transmission electron microscopy (STEM) at 200 kV equipped with an energy dispersive spectrometer (EDS) for acquiring compositions and high-spatial resolution elemental maps, scanning electron microscopy (SEM) also combined with EDS, and electron probe microanalysis (EPMA) equipped with wavelength dispersive spectrometers (WDS). (Not all samples were subject to the entire aforementioned range of analytical techniques.) AES spectra were acquired at 20 keV incident electron energy using a PHI 680 Scanning Auger Nanoprobe. AES depth profiles were obtained by sputtering with Ar+ ions at an incident angle of 45° from the surface normal. In the profiles shown in this paper, two different sputter rates were used: for as-received Fe–20Cr–4V sheet the sputter rate was 2 nm min^{-1} (achieved with 2 kV Ar ions) due to the thinness of the native oxide layer; for all other profiles the sputter rate was 84 nm min^{-1} (using 3 kV Ar ions). Sputter rates were determined in separate experiments using 100 nm thick SiO_2 standard films. Compositions shown in the profiles were determined using tabulated Auger sensitivity factors from the PHI MultiPak (v.6.0) Analysis software. Deconvolution of the Cr Auger signals into oxide, nitride, or metal was accomplished using a linear-least squares fitting routine contained in the MultiPak software. The basis spectra used for fitting were taken from regions within the profile identified as nitride-rich, oxide-rich and metal-rich. Thin specimens for imaging and microanalysis in the STEM were prepared in cross-section from the bulk samples by focused ion beam (FIB) milling.

ICR values were obtained using two pieces of conductive carbon paper that were sandwiched between the coupon faces and two copper plates. The total resistance was measured as a function of contact pressure, and corrections were made for the resistance of the carbon paper/copper plate interfaces ($R_{C/Cu}$) by calibration. For samples examined after corrosion exposure, in which only one coupon face was exposed to the test environment, the calculated ICR values were not divided by two and thus represent both sets of carbon paper/nitride interfaces. For simplicity these values are referred to as 2 × ICR, and all data, both as-received and after corrosion are plotted as 2 × ICR. Further details of the ICR measurement technique are provided in Ref. [11].

Corrosion behavior was evaluated by static polarization in a simulated highly aggressive PEMFC environment, consisting of 1 M H_2SO_4 + 2 ppm F^- solution at 70 °C, purged either with H_2 gas to simulate the PEMFC anode environment or air to simulate the PEMFC cathode environment. A piece of Pt sheet/foil served as the counter electrode and a saturated calomel electrode was used as the reference. In these measurements, the samples were stabilized at open circuit (E_{corr}) for 5 min, and then a specific potential was applied and held for 7.5 h and the current–time curve was recorded. Two potentials were chosen for the tests: +0.14 V vs SHE for the anode conditions, and +0.84 V vs SHE for the cathode conditions. All voltages in this paper are presented relative to the standard hydrogen electrode (SHE).

3. Results and discussion

3.1. Pre-oxidation and nitridation processing overview

Table 2 shows specific reaction conditions and O/N mass uptake for each sample reported in Figs. 1–10. All samples showed some degree of internal nitridation. Nitridation mass uptakes of <0.2–0.4 mg cm^{-2} were generally found to correlate well with suf-

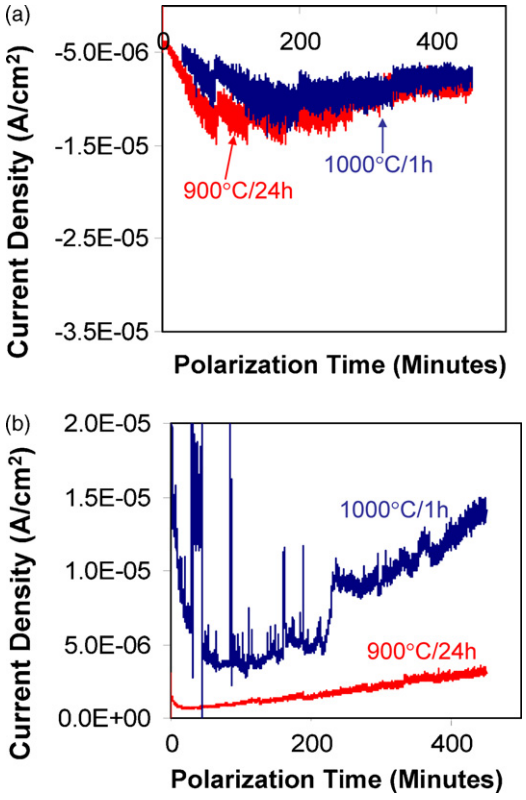

Fig. 1. Static polarization data for 925 °C/2 h pre-oxidized Fe–20Cr–4V sheet coupon samples nitrided 1000 °C/1 h (blue) or 900 °C/24 h (red) (further details in Table 2) in 1 M H_2SO_4 + 2 ppm F^- at 70 °C. (a) H_2-purged simulated anode conditions at +0.14 V vs SHE and (b) aerated simulated cathode conditions held at +0.84 V vs SHE. Note that the first 30 min of data for the 1000 °C/1 h nitrided sample were omitted from the plot due to excessive noise scatter.

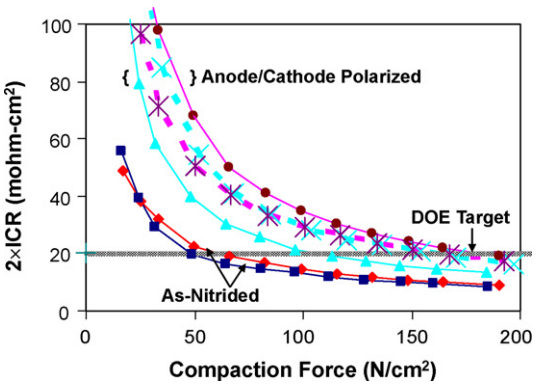

Fig. 2. 2 × ICR vs compaction force curves for 925 °C/2 h pre-oxidized Fe–20Cr–4V sheet coupon samples as-nitrided 1000 °C/1 h (blue) or 900 °C/24 h (red) (further details in Table 2). Polarized data is after simulated anode (solid line) or cathode side (dashed line) conditions (current density data shown in Fig. 1): 1000 °C/1 h nitrided (light blue) and 900 °C/24 h nitrided (pink).

ficiently limited internal nitridation to prevent significant alloy embrittlement, with levels of <0.2 mg cm^{-2} preferred.

3.2. Pre-oxidized and nitrided Fe–20Cr–4V sheet coupon polarization and ICR

Sheet coupons of Fe–20Cr–4V were treated using the same pre-oxidation condition (2 h at 925 °C in flowing N_2–4H_2–0.5O_2) and two different nitridation conditions, either 1000 °C/1 h or 900 °C/24 h in flowing/scrubbed N_2–4H_2 (Table 2). The 1000 °C/1 h condition is of particular interest as the shorter the nitriding cycle, the lower the cost. Specific mass changes, which reflect the total uptake of O or N, were ~0.22–0.23 mg cm^{-2} on pre-oxidation. The 900 °C/24 h treatment yielded an additional 0.18 mg cm^{-2} uptake on nitridation, whereas the 1000 °C/1 h treatment yielded an additional 0.06 mg cm^{-2} uptake.

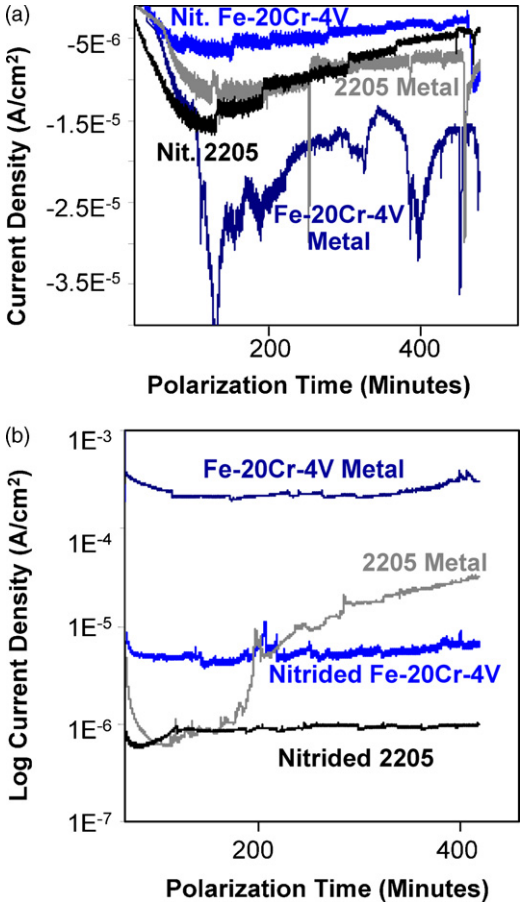

Fig. 3. Static polarization data for Fe–20Cr–4V and 2205 foils untreated (metal) and after 900 °C/2 h pre-oxidation and 1000 °C/2 h nitridation (further details in Table 2). (a) H_2-purged simulated anode conditions at +0.14 V vs SHE and (b) aerated simulated cathode conditions at +0.84 V vs SHE.

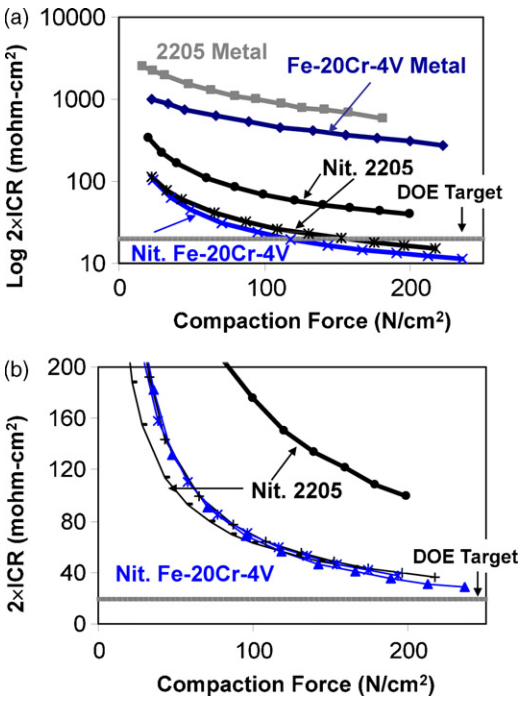

Fig. 4. 2 × ICR vs compaction force curves. (a) Fe–20Cr–4V and 2205 foils untreated (metal) and after 900 °C/2 h pre-oxidation and 1000 °C/2 h nitridation; (b) pre-oxidized and nitrided Fe–20Cr–4V and 2205 foils after polarization under simulated anode and cathode conditions (current density data shown in Fig. 3, further details in Table 2). The after polarization values were essentially the same for pre-oxidized and nitrided Fe–20Cr–4V and 2205 under both anode and cathode conditions. The high 2 × ICR value nitrided 2205 foil from Fig. 4a is shown after anode polarization in Fig. 4 (highest curve shown in Fig. 4b).

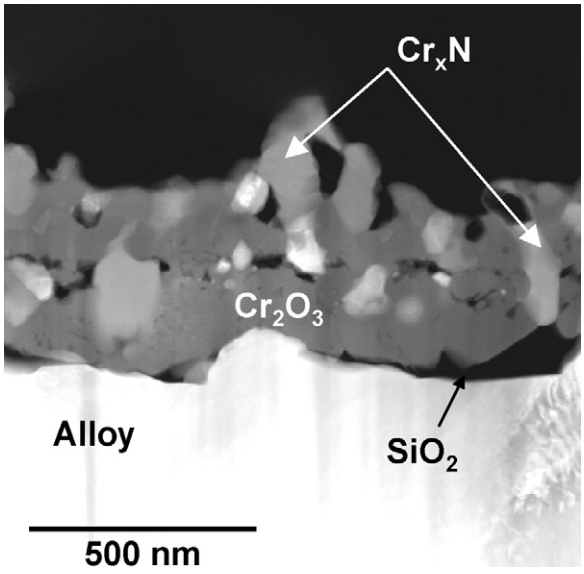

Fig. 5. Cross-section to HAADF-STEM image of 900 °C/30 min pre-oxidized and 1000 °C/2 h nitrided 2205 stainless steel foil (cathode polarized sample shown in Figs. 3b and 4b, further details in Table 2).

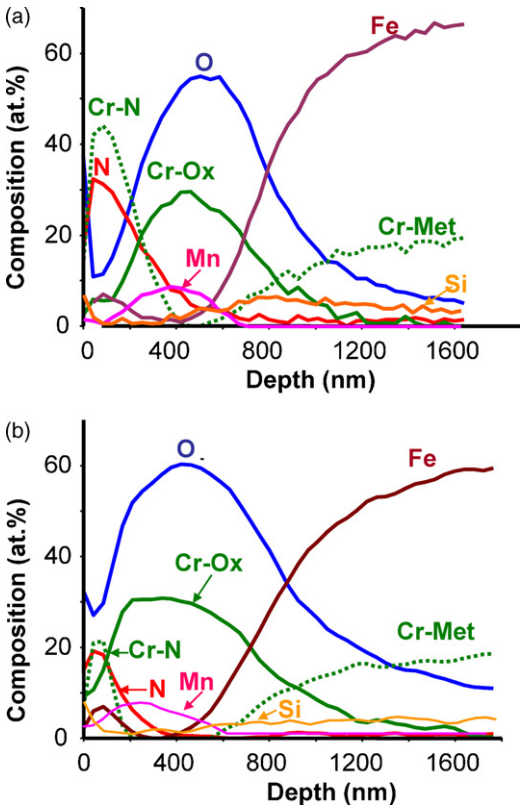

Fig. 6. AES data for pre-oxidized and nitrided 2205 stainless steel foil (further details in Table 2) showing range of surface chemistries observed after nominally similar reaction conditions. (a) N-rich; (b) O-rich. Note that adventitious C was also present at the surface, data not included in above plots. The Cr data was deconvoluted into Cr-oxygen and Cr-metal/nitrogen curves.

Static polarization curves under simulated highly-aggressive PEMFC bipolar plate conditions using 1 M sulfuric acid + 2 ppm F^- at 70 °C are shown in Fig. 1 for simulated anode-side conditions at +0.14 V and H_2 sparging (Fig. 1a) and simulated cathode-side conditions at +0.84 V and air sparging (Fig. 1b). The curves under the simulated anodic conditions were essentially the same

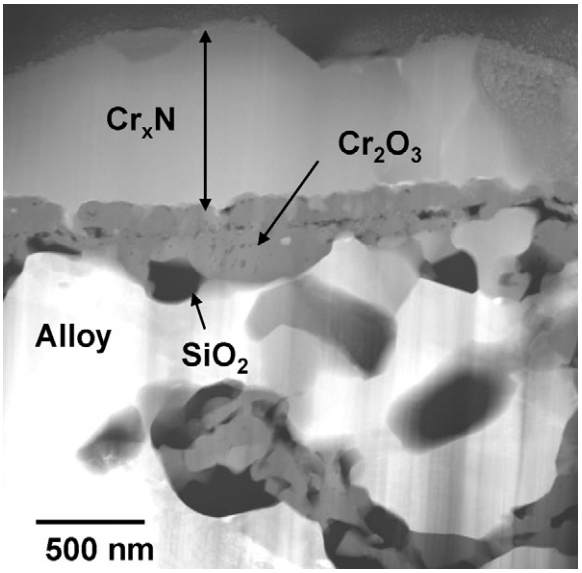

Fig. 7. Cross-section to HAADF-STEM image of 900 °C/15 min pre-oxidized and 1000 °C/4 h nitrided 2205 stainless steel foil (further details in Table 2).

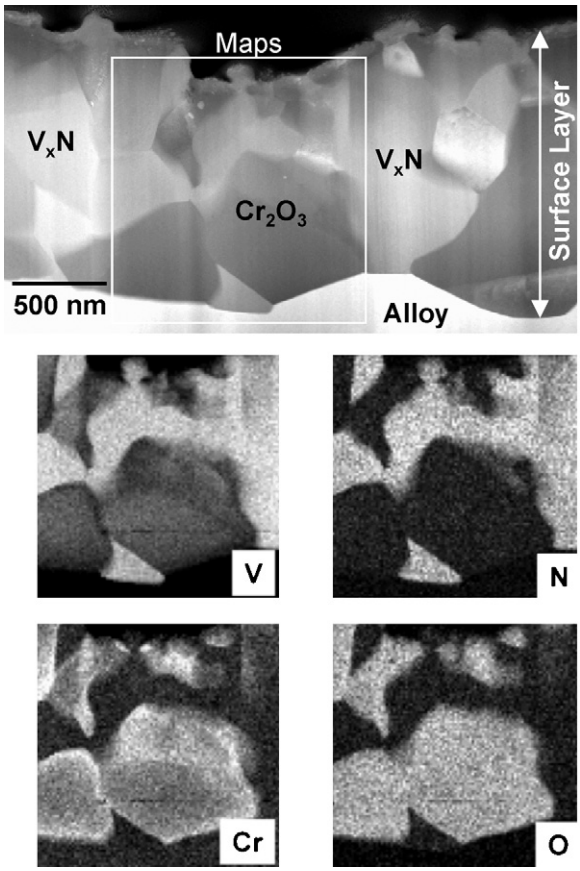

Fig. 8. Cross-section to HAADF-STEM image and elemental maps for 925 °C/2 h pre-oxidized and 1000 °C/4 h nitrided Fe–20Cr–4V sheet coupon (further details in Table 2). This particular sample was polarized under simulated anodic conditions and yielded a current density of ~6×10^{-6} A cm^{-2} after 7.5 h polarization (same conditions and similar behavior to pre-oxidized/nitrided Fe–20Cr–4V sheet coupon results shown in Fig. 1a).

for the two treatment conditions, and reached a limiting value of −6 to 8×10^{-6} A cm^{-2} after 7.5 h (450 min) of polarization. These values are comparable to/moderately higher than the −1 to -6×10^{-6} A cm^{-2} range current densities observed for nitrided high-Cr Ni–Cr (30–50 wt.% Cr) and Fe–Cr (27–29 wt.% Cr) alloys previously studied under this test condition [19–22]. Under simulated aggressive cathodic conditions, the 1000 °C/1 h treatment yielded higher (worse) current densities, 14×10^{-6} A cm^{-2} after 7.5 h vs 3×10^{-6} A cm^{-2} for the 900 °C/24 nitrided sample. Current densities for nitrided high-Cr Ni–Cr and Fe–Cr alloys previously studied under this test condition were typically in the range of $1–2 \times 10^{-6}$ A cm^{-2} [19–22]. The moderate increase in current density with time observed under the simulated cathodic conditions (Fig. 1b) is not uncommon in static polarization curves for nitrided stainless steel surfaces under these test conditions, and is suggestive of a minor degree of susceptibility to surface attack. It is considered a consequence of the 1 M sulfuric acid + 2 ppm F^- test solution, which is far more aggressive than the environment expected under stable fuel cell operating environments (~pH 3 sulfuric acid and lower levels of F^-) [1–10].

As-nitrided ICR values for Fe–20Cr–4V sheet after the two different nitridation conditions were similar (Fig. 2) and met the USDOE target of <20 mΩ cm^2 at loads of ~150–200 N cm^{-2}. Note that Fig. 2 effectively plots ~2× the ICR value as it includes both top and bottom coupon/carbon paper interfaces. This convention was adopted because only one coupon face was exposed in polarization testing, which means that ICR values obtained after polarization included both polarized and un-exposed faces. The USDOE target was also

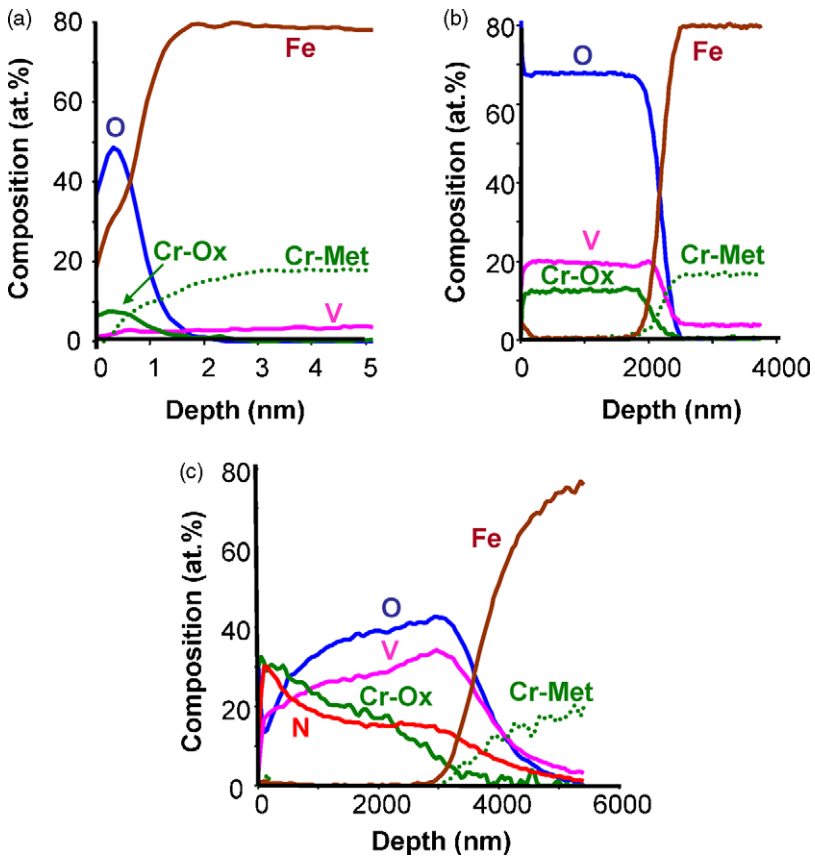

Fig. 9. AES data for Fe–20Cr–4V sheet coupons. (a) As-received; (b) after 900 °C/2 h pre-oxidation; (c) after 900 °C/2 h pre-oxidation and 1000 °C/2 h nitridation. Further details in Table 2. Note that adventitious C was also present at the surface (data not included in above plots). The Cr data was deconvoluted into Cr-oxygen and Cr-metal/nitrogen curves.

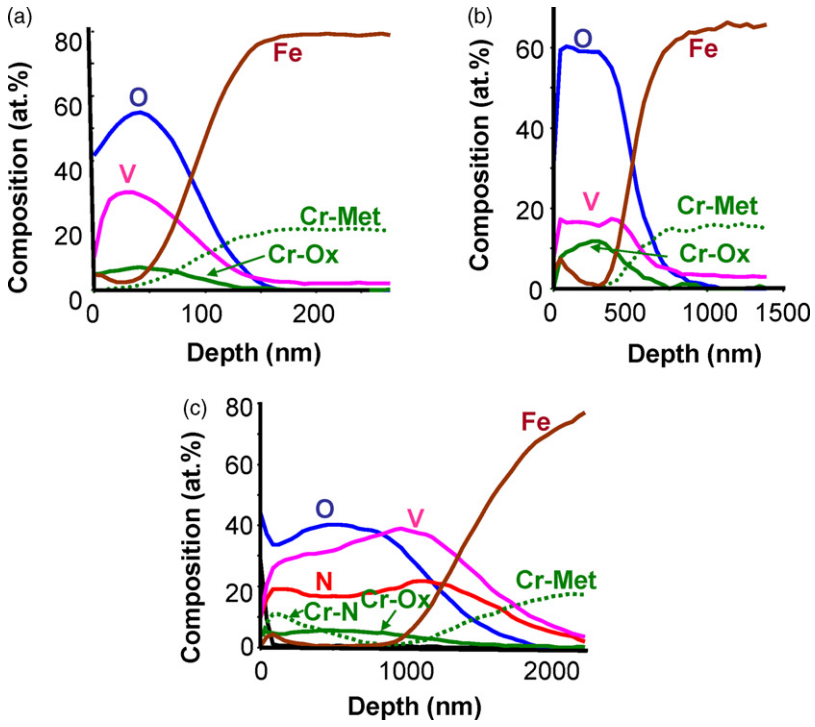

Fig. 10. AES data for Fe–20Cr–4V foil. (a) As-received; (b) after 900 °C/1 h pre-oxidation; (c) after 900 °C/1 h pre-oxidation and 1000 °C/2 h nitridation. Further details in Table 2. Note that adventitious C was also present at the surface (data not included in above plots). The Cr data was deconvoluted into Cr-oxygen and Cr-metal/nitrogen curves.

doubled from <10 mΩ cm^2 to <20 mΩ cm^2 for consistency with this convention. Untreated stainless steels typically exhibit as-received ICR values an order of magnitude higher than the USDOE target and the values obtained for the nitrided Fe–20Cr–4V [9,11]. An increase in ICR was observed on polarization of the nitrided Fe–20Cr–4V, similar to that reported for nitrided high-Cr Fe–Cr alloys previously studied [19,21,22]; however, as with the high-Cr Fe–Cr alloys, the increase remained within the USDOE target. Interestingly, the higher current density reported for the 1000 °C/1 h treated material under simulated aggressive cathodic conditions did not result in a greater increase in ICR after polarization than the 900 °C/24 h nitridation conditions.

3.3. Pre-oxidized and nitrided Fe–20Cr–4V and 2205 foil polarization and ICR

Fig. 3 shows static polarization curves in 1 M sulfuric acid + 2 ppm F^- at 70 °C for 0.1 mm thick foils of Fe–20Cr–4V and 2205 stainless steel, both as-received (no surface treatment) and after pre-oxidation (900 °C, 2 h N_2–4H_2–0.5O_2) and nitridation (1000 °C/2 h scrubbed N_2–4H_2) (Table 2). The untreated Fe–20Cr–4V foil exhibited relatively poor behavior under simulated anodic conditions (Fig. 3a) with current densities in the range of -20×10^{-6} A cm^{-2}. In contrast, the untreated 2205 stainless steel foil exhibited a current density in the -8×10^{-6} A cm^{-2} range after 7.5 h static polarization under simulated anodic conditions. Both Fe–20Cr–4V and 2205 foils exhibited significant reduction in current densities after the pre-oxidation/nitridation treatment, with values approaching -3×10^{-6} A cm^{-2} and -4×10^{-6} A cm^{-2}, respectively, after 7.5 h static polarization.

Similar trends were observed under simulated cathode-side conditions, with the pre-oxidation and nitridation treatments yielding significant improvements (reduction) in current densities. (A logarithmic scale is used for current density in Fig. 3b to better plot the entire range of data observed.) The pre-oxidized and nitrided 2205 foil exhibited current densities of only 1×10^{-6} A cm^{-2}, which is in the range of nitrided high-Cr Ni–Cr (30–50 wt.% Cr) and Fe–Cr (27–29 wt.% Cr) alloys previously studied [19–22]. The pre-oxidized and nitrided Fe–20Cr–4V foil exhibited moderately higher current densities, in the range of 6×10^{-6} A cm^{-2} after 7.5 h of static polarization.

Fig. 4a shows ICR data for untreated and pre-oxidized and nitrided Fe–20Cr–4V and 2205 stainless steel foils (900 °C, 2 h N_2–4H_2–0.5O_2 and 1000 °C/2 h scrubbed N_2–4H_2, respectively). The untreated foils yielded ICR values ~20–30 times higher than the USDOE target of <20 mΩ cm^2 at loads of ~150–200 N cm^{-2}, consistent with reported value ranges [11] for stainless steel sheet material. In contrast, the pre-oxidized and nitrided Fe–20Cr–4V foil exhibited a 2 × ICR value of ~15 mΩ cm^2 at 150 N cm^{-2}, which was slightly higher than that observed for pre-oxidized and nitrided Fe–20Cr–4V sheet material (Figs. 2 and 4a), but nonetheless meets the USDOE target. Run-to-run scatter was observed for the pre-oxidized and nitrided 2205 stainless steel foil, with values ranging from 20 to 50 mΩ cm^2 at 150 N cm^{-2}.

ICR values after polarization for pre-oxidized and nitrided Fe–20Cr–4V and 2205 stainless steel foil (data from Fig. 3) are shown in Fig. 4b. The 2 × ICR vs compaction force curves were essentially identical for Fe–20Cr–4V and 2205 stainless steel foils after static polarization under both anode-side and cathode-side conditions, with 2 × ICR values in the range of 40–50 mΩ cm^2 at 150 N cm^{-2}. These resulting ICR values were approximately twice those observed for pre-oxidized and nitrided Fe–20Cr–4V sheet material after similar polarization (Fig. 2), and exceeded the USDOE ICR target by a factor of 2–2.5. Although these results indicate a lower level of performance by the pre-oxidized and nitrided Fe–20Cr–4V foil, it should be noted that the 1 M H_2SO_4 + 2 ppm F^- test environment used in the present work was much more aggressive than that expected in an operating fuel cell environment, such that similar ICR increases may not occur in actual fuel cell service. Immersion polarization testing may also represent a more severe condition than actual in-cell fuel cell service, as complete liquid immersion is akin to a flooded fuel cell, which in itself represents a significantly degraded fuel cell operational state. Also shown in Fig. 4b are ICR data for the high ICR pre-oxidized and nitrided 2205 (Fig. 4a) after polarization under simulated anode-side conditions (Table 2). This sample showed a significant increase in the 2 × ICR value, from ~50 to ~125 mΩ cm^2 at 150 N cm^{-2}, despite exhibiting a relatively low current density of -2×10^{-6} A cm^{-2} after 7.5 h of polarization (polarization curve not shown).

3.4. Microstructure and surface chemistry

Pre-oxidation and nitridation of 2205 stainless steel foil resulted in a highly heterogeneous and varied range of surface structures (Figs. 5 and 6). A high-angle annular dark field (HAADF) cross-section image for the cathode polarized sample (Figs. 3b and 4) is shown in Fig. 5. The surface consisted of Cr_xN (x = 1,2) particles dispersed in Cr_2O_3, with some local regions of SiO_2 at the alloy/layer interface (phase identification based primarily on EDS/WDS data). In most regions the Cr_xN did not appear to be continuous from the surface into the alloy (little through-layer thickness continuity). Fig. 6 shows a representative range of surface chemistries obtained after pre-oxidation and nitridation of 2205 stainless steel foil under conditions similar to that used for the sample shown in Fig. 5 (Table 2). The surface chemistries obtained by AES were consistent with the cross-section structure observed by STEM, Cr_xN and Cr_2O_3, but with significant variability in the relative amounts of oxide/nitride at the surface. Chromia exhibits poor electrical conductivity, and it is likely that the near-continuous nature of the Cr_2O_3 was responsible for the variability of ICR values observed for pre-oxidized and nitrided 2205 stainless steel foil (Fig. 4). It is also possible that preferential electrical conduction across the Cr-nitride rich surface, as opposed to through-thickness conduction, may have contributed to the relatively low ICR values obtained for pre-oxidized and nitrided 2205 stainless steel foil, i.e. the functional values of ICR may effectively be higher than those measured (issue discussed in Ref. [9]). For example, the material shown in Fig. 6b was resistive when evaluated by a multi-probe (and hence was not measured for ICR), consistent with its very low mass gain on nitridation of 0.005 mg cm^{-2} (Table 2). The reacted surfaces formed on 2205 stainless steel foil were, however, very rich in Cr, with only small amounts of Fe or Mn (Fig. 6). The good corrosion resistance observed for surface treated 2205 foil (Fig. 3) is attributed to this Cr-rich surface chemistry. The segregation of Mn and Si to the reacted surface layer is consistent with their greater thermodynamic stability over that of Cr in oxygen.

Fig. 7 shows the results of an attempt to improve the continuity of Cr_xN in 2205 stainless steel foil by decreasing the pre-oxidation stage to 900 °C/15 min and increasing the nitridation stage to 1000 °C/4 h in conjunction with a 400 °C/12 h vacuum bake out prior to nitridation (Table 2). Continuous surface Cr_xN was formed under these conditions, however, a near continuous Cr_2O_3 layer, with local regions of SiO_2 at the alloy/layer interface (as well as some internal nitridation of Cr) was still observed beneath the surface Cr_xN layer. Such a structure may exhibit good corrosion resistance and surface conductivity, but would not be expected to exhibit sufficient through-thickness conductivity to function as a bipolar plate.

A HAADF-STEM image of a typical cross-section structure formed on pre-oxidized and nitrided Fe–20Cr–4V is shown in Fig. 8 for a sheet coupon of Fe–20Cr–4V pre-oxidized for 2 h at

925 °C in N_2–$4H_2$–$0.5O_2$ and nitrided for 4 h at 1000 °C in flowing scrubbed N_2–$4H_2$ (Table 2). The surface structure consisted primarily of intermixed Cr_2O_3 and V_xN. Cr_xN surface particles were also observed, but not retained in the cross-section region shown in Fig. 8 (phase identification based on elemental maps and XRD results for similarly treated samples). Some internal nitridation, primarily as V_xN, was also present (not shown in Fig. 8). In contrast to the pre-oxidized and nitrided 2205 material, the Fe–20Cr–4V material formed through-layer thickness nitrides, which likely accounts for its lower, more consistent ICR values. Similar structures containing through-thickness V_xN were also observed in pre-oxidized and nitrided Fe–20Cr–4V foils, although there was some scatter in the relative amounts of oxide vs nitride. Sheet coupon material generally exhibited a greater proportion of through-thickness nitride than did foil material, despite similar pre-oxidation and nitridation processing steps.

Figs. 9 and 10 show surface chemistry as a function of depth determined by AES for representative Fe–20Cr–4V sheet coupon and foil material as-received, after pre-oxidation (1 or 2 h at 900 °C in flowing N_2–$4H_2$–$0.5O_2$) and pre-oxidation and nitridation (2 h at 1000 °C in flowing scrubbed N_2–$4H_2$) (Table 2). The native oxide surface on the sheet coupon material was <~4 nm thick and rich in Fe, whereas the native oxide layer on the foil was ~150 nm thick (i.e. it contained remnant oxide from the heat treatment) and rich in V (Figs. 9a and 10a). On pre-oxidation (Figs. 9b and 10b), both sheet and foil material formed X_2O_3 based surfaces (X = Cr, V) ~1000–2000 nm thick, which overwhelmed the thinner, as-received native oxide surface layers. Iron was present in both surfaces, with approximately 5 atomic percent (at.%) detected at the sheet material surface and 8 at.% in the foil surface. The Fe–20Cr–4V sheet material tended to form a thicker oxide, with lower Fe surface content, than foil material under most pre-oxidation conditions examined, although it is noted that for the case of the AES data shown in Figs. 9a and 10a the sheet material had the longer pre-oxidation treatment.

Figs. 9c and 10c show pre-oxidized material from the same batches as shown in Figs. 9b and 10b after nitridation for 2 h at 1000 °C in flowing, scrubbed N_2–$4H_2$ (note that the foil and sheet samples were treated in different furnace batch runs) (Table 2). Consistent with the STEM cross-sections, the sheet material generally exhibited higher levels of nitrogen and lower levels of oxygen at the surface after pre-oxidation and nitridation. Both surfaces were very rich in Cr and V, with virtually no Fe in the sheet coupon surface layer but ~3–4 at.% retained Fe in the foil coupon surface layer. The higher O levels and small amount of retained Fe in the surface of the nitrided Fe–20Cr–4V foil likely accounts for its higher initial ICR values than the sheet material (Fig. 4).

The mechanism behind the greater enrichment of nitrogen in the Fe–20Cr–4V sheet material surfaces compared to foil under ostensibly similar conditions is not understood. The sheet material was coarse grained (>100 micron grain size) compared to the 0.1 mm thick foil, which had an order of magnitude finer grain size. These grain size differences could potentially affect outward transport of Cr and V to the surface layer, although the pre-oxidized surface chemistries were similar and the 900–1000 °C reaction temperatures are sufficiently hot that alloy grain boundary transport would not be expected to control alloy diffusion. There were also differences in surface finish, as the sheet material was polished to a uniform surface finish using #240 grit SiC paper, while the foil was treated in the as-processed foil condition, albeit after a light abrasive surface scrubbing to remove the remnant heat treatment oxide formed during foil production. There were differences in the amount of Fe in the pre-oxidized sheet and foil surfaces, with greater retention of this Fe after nitridation of foil than sheet, which does suggest possible differences in surface layer or alloy transport properties between foil and sheet.

3.5. Implications for bipolar plates

Previous efforts using model high-Cr, Ni–Cr and Fe–Cr base alloys treated in static N_2–$4H_2$ mixtures with oxygen impurities yielded continuous Cr-nitride base surface layers with low and stable ICR values and excellent corrosion resistance in simulated PEMFC environments [9,17–22,43]. The lower alloy Cr and V levels and use of short, distinct pre-oxidation and nitridation steps, which were taken to meet bipolar plate cost and production targets, resulted in a fundamentally different surface structure. Instead of continuous Cr-nitride, the Fe–20Cr–4V material yielded V_xN dispersed in chromia (Fig. 8). From a thermodynamic perspective this is not surprising as V is far more stable in nitrogen than is Cr [22]. This nitride/oxide structure was somewhat reminiscent of the NMPOL surfaces formed on high-Cr superferritic alloys 446 MOD-1 or AL29-4C® [19,21]. The resultant ICR values and corrosion resistance for the pre-oxidized and nitrided Fe–20Cr–4V foil, although not quite as good as earlier work with model materials and lab scale conditions, still yielded significant improvements over that of untreated stainless steel foils.

In contrast, although good corrosion resistance was achieved for pre-oxidized and nitrided 2205 stainless steel foil, there was significant sensitivity to oxygen impurities in the nitriding environment resulting in scatter of ICR values, attributed primarily to the retention of near-continuous chromia in the surface layer (possibly contributed to by local regions of SiO_2). Single-cell fuel cell testing of stamped and pre-oxidized/nitrided Fe–20Cr–4V and 2205 stainless steel foils (presented in part 2 of this paper, Ref. [41]) were consistent with the findings of the present work, with excellent initial single-cell behavior exhibited by treated Fe–20Cr–4V stamped foils and poor behavior of treated 2205 stamped foils, ostensibly due to the pockets of continuous oxide formation (see Ref. [41] for further details). The structure of the pre-oxidized and nitrided surface on the Fe–20Cr–4V, and to some extent that of earlier work with 446 MOD-1 or AL29-4C® [19,22], suggests that additions of strong nitride-forming elements such as Ti (and of course V [9,22]) aid in conversion of oxide to nitride and tend to yield the through-layer thickness nitride particles needed for bipolar plate applications. This would suggest future selection of commercially available stainless steel alloy foils containing Ti additions, types 444 and 321 for example, in addition to continued work on developmental Fe–Cr–V alloy foils. Such Ti additions are frequently used to provide high-temperature strength in heat-resistant stainless steel grades. Stainless steel grades that are also nitrogen stabilized may also be of interest as residual nitrogen in the alloy may slow undesirable inward nitrogen transport and internal nitridation by reducing the nitrogen gradient into the alloy.

In addition to long term single-cell durability testing of stamped and pre-oxidized/nitrided foils [41], future efforts will examine consolidation of the discrete bake out, pre-oxidation, and nitridation steps to a single continuous process. Even with the V containing alloys, some concerns remain regarding the ability to sufficiently control oxygen impurities in the nitriding environment in large-scale production. Also of interest is the use of faster nitridation heating and cooling rates, which could shorten cycle time (and therefore cost), as well as potentially permit the use of high-Cr superferritic alloys by eliminating the potential for brittle sigma phase formation during the surface treatment. It will need to be demonstrated that such high-Cr alloys are sufficiently amenable to stamping in foil form. Other scale up and cost considerations include the level of Mn and Si impurities in the alloy, which as shown for 2205 stainless steel can segregate to the reaction layer and potentially degrade properties. The present work suggests that as more commercially viable compositions and pre-oxidation/nitridation conditions are used, the ICR and corrosion resistance properties of the surface will be compromised relative

to results obtained under model conditions. Further study will be needed to determine if the resultant surfaces, although not as good as the model materials, may still be sufficiently high-performing for commercial use. The results of single-cell fuel cell studies of stamped and pre-oxidized/nitrided stainless steel foils are presented in part 2 of this paper [41]. In this testing, stamped and pre-oxidized/nitrided Fe–20Cr–4V exhibited behavior comparable to that of benchmark graphite plates, which indicates the potential of the pre-oxidation and nitridation approach to meet USDOE targets.

4. Summary and conclusions

(1) Pre-oxidation and nitridation of Fe–20Cr–4V and 2205 stainless steel foils yielded 10^{-6} A cm^{-2} range current densities on polarization in 1 M H_2SO_4 + 2 ppm F^- solution at 70 °C, purged either with H_2 gas to simulate PEMFC anode environment or air to simulate the PEMFC cathode environment. This relatively low level of current densities approached those previously observed for nitrided model and commercial Ni–Cr alloys, which showed good behavior in subsequent single-cell fuel cell testing [9,18,19].

(2) As pre-oxidized and nitrided ICR values for Fe–20Cr–4V and 2205 stainless steel generally met USDOE targets, and were over an order of magnitude range lower than untreated alloy foils. Some scatter and out of USDOE target range ICR values were observed with the pre-oxidized and nitrided 2205. On polarization, ICR values for pre-oxidized and nitrided Fe–20Cr–4V and 2205 foils increased ~2–2.5 times.

(3) The pre-oxidized and nitrided surface structures consisted primarily of intermixed Cr_2O_3 and V_xN for Fe–20Cr–4V. A key finding was the tendency for through-thickness V_xN formation, which is believed to aid attainment of low ICR values. In contrast, Cr_2O_3 and Cr_xN formation was observed for 2205 stainless steel foils in which the Cr_2O_3 was near continuous. The variability in ICR values obtained for pre-oxidized and nitrided 2205 stainless steel was attributed to the Cr_2O_3 continuity.

(4) Stainless steel alloy foils containing strong nitride-forming additions such as V and Ti are of interest for surface treatment by pre-oxidation and nitridation to achieve electrically conductive and corrosion-resistant surface layers of interest for fuel cells, batteries, and sensors.

Acknowledgements

The authors thank D.F. Wilson, T.J. Toops, B.A. Pint, and D.P. Stinton for reviewing this manuscript. The authors also thank L.R. Walker for microprobe analysis, D.W. Coffey for STEM specimen preparation, G.W. Garner for performing the nitridation exposures, and J.M. Rakowski of ATI Allegheny Ludlum for the Fe–20Cr–4V and 2205 stainless steel foils. Funding from the U.S. Department of Energy's Hydrogen, Fuel Cells, and Infrastructure Program is gratefully acknowledged. Research supported by ORNL's SHaRE User Facility, which is sponsored by the Scientific User Facilities Division, Office of Basic Energy Sciences, the U.S. Department of Energy. B. McCarthy thanks the ORAU HERE program for a summer internship at ORNL. ORNL is managed by UT-Battelle, LLC for the US DOE under contract DE-AC05-00OR22725. Notice: This submission was sponsored by a contractor of the United States Government under contract DE-AC05-00OR22725 with the United States Department of Energy. The United States Government retains, and the publisher, by accepting this submission for publication, acknowledges that the United States Government retains, a nonexclusive, paid-up, irrevocable, worldwide license to publish or reproduce the published form of this submission, or allow others to do so, for United States Government purposes.

References

[1] V. Mehta, J.S. Cooper, J. Power Sources 114 (1) (2003) 32–53.
[2] A. Hermann, T. Chaudhuri, P. Spagnol, Int. J. Hydrogen Energy 30 (12) (2005) 1297–1302.
[3] H. Tawfik, Y. Hung, D. Mahajan, J. Power Sources 163 (2) (2007) 755–767.
[4] E. Middelman, W. Kout, B. Vogelaar, J. Lenssen, E. de Waal, J. Power Sources 118 (1–2) (2003) 44–46.
[5] Y.Y. Shao, G.P. Yin, Z.B. Wang, Y.Z. Gao, J. Power Sources 167 (2) (2007) 235–242.
[6] N.D.L. Heras, E.P.L. Roberts, R. Langton, D.R. Hodgson, Energy Environ. Sci. 2 (2) (2009) 206–214.
[7] J.F. Wu, X.Z. Yuan, J.J. Martin, H.J. Wang, J.J. Zhang, J. Shen, S.H. Wu, W. Merida, J. Power Sources 184 (1) (2008) 104–119.
[8] X.Z. Yuan, H.J. Wang, J.J. Zhang, D.P. Wilkinson, J. New Mater. Electrochem. Syst. 8 (4) (2005) 257–267.
[9] M.P. Brady, B. Yang, H. Wang, J.A. Turner, K.L. More, M. Wilson, F. Garzon, JOM-J. Met. Miner. Mater. Soc. 58 (August (8)) (2006) 50–57.
[10] D.P. Davies, P.L. Adcock, M. Turpin, S.J. Rowen, J. Power Sources 86 (1–2) (2000) 237–242.
[11] H.L. Wang, G. Teeter, J. Turner, J. Electrochem. Soc. 152 (3) (2005) B99–B104.
[12] J. Wind, R. Spah, W. Kaiser, G. Bohm, J. Power Sources 105 (2) (2002) 256–260.
[13] R.C. Makkus, A.H.H. Janssen, F.A. de Bruijn, R.K.A.M. Mallant, J. Power Sources 86 (1–2) (2000) 274–282.
[14] A. Pozio, R.F. Silva, M. De Francesco, L. Giorgi, Electrochim. Acta 48 (11) (2003) 1543–1549.
[15] H.L. Wang, J.A. Turner, J. Power Sources 183 (2) (2008) 576–580.
[16] R. Borup, N.E. Vanderborgh, in: D.H. Doughty, B. Vyas, T. Takamura, J.R. Huff (Eds.), Mat Res. Soc. Symp. Proc. 393, Material Research Society, Pittsburgh, PA, USA, 1995, p. 151.
[17] M.P. Brady, K. Weisbrod, C. Zawodzinski, I. Paulauskas, R.A. Buchanan, L.R. Walker, Electrochem. Solid-State Lett. 5 (11) (2002) A245–A247.
[18] M.P. Brady, K. Weisbrod, I. Paulauskas, R.A. Buchanan, K.L. More, H. Wang, M. Wilson, F. Garzon, L.R. Walker, Scripta Mater. 50 (7) (2004) 1017–1022.
[19] M.P. Brady, H. Wang, B. Yang, J.A. Turner, M. Bordignon, R. Molins, M. Abd Elhamid, L. Lipp, L.R. Walker, Int. J. Hydrogen Energy 32 (16) (2007) 3778–3788.
[20] H. Wang, M.P. Brady, J.A. Turner, J. Power Sources 138 (1–2) (2004) 86–93.
[21] H. Wang, M.P. Brady, K.L. More, H.M. Meyer, J.A. Turner, J. Power Sources 138 (1–2) (2004) 75–85.
[22] B. Yang, M.P. Brady, H. Wang, J.A. Turner, K.L. More, D.J. Young, P.F. Tortorelli, E.A. Payzant, L.R. Walker, J. Power Sources 174 (1) (2007) 228–236.
[23] H.S. Choi, D.H. Han, W.H. Hong, J.J. Lee, J. Power Sources 189 (2) (2009) 966–971.
[24] D.H. Han, W.H. Hong, H.S. Choi, J.J. Lee, Int. J. Hydrogen Energy 34 (5) (2009) 2387–2395.
[25] J. Liu, F. Chen, Y.G. Chen, D.M. Zhang, J. Power Sources 187 (2) (2009) 500–504.
[26] Y. Fu, G.Q. Lin, M. Hou, B. Wu, H.K. Li, L.X. Hao, Z.G. Shao, B.L. Yi, Int. J. Hydrogen Energy 34 (1) (2009) 453–458.
[27] H.Y. Lee, S.H. Lee, J.H. Kim, M.C. Kim, D.M. Wee, Int. J. Hydrogen Energy 33 (15) (2008) 4171–4177.
[28] A. Pozio, F. Zaza, A. Masci, R.F. Silva, J. Power Sources 179 (2) (2008) 631–639.
[29] W. Yoon, X.Y. Huang, P. Fazzino, K.L. Reifsnider, M.A. Akkaoui, J. Power Sources 179 (1) (2008) 265–273.
[30] D.G. Nam, H.C. Lee, J. Power Sources 170 (2) (2007) 268–274.
[31] R.F. Silva, A. Pozio, J. Fuel Cell Sci. Technol. 4 (2) (2007) 116–122.
[32] R.F. Silva, D. Franchi, A. Leone, L. Pilloni, A. Masci, A. Pozio, Electrochim. Acta 51 (17) (2006) 3592–3598.
[33] M. Kumagai, S.T. Myung, R. Asaishi, Y.K. Sun, H. Yashiro, Electrochim. Acta 54 (2) (2008) 574–581.
[34] R.J. Tian, J.C. Sun, J.L. Wang, Int. J. Hydrogen Energy 33 (24) (2008) 7507–7512.
[35] C.X. Shan, X. Hou, K.L. Choy, P. Choquet, Surf. Coat. Technol. 202 (10) (2008) 2147–2151.
[36] Y. Wang, D.O. Northwood, Int. J. Hydrogen Energy 32 (7) (2007) 895–902.
[37] Y. Wang, D.O. Northwood, J. Power Sources 165 (1) (2007) 293–298.
[38] K.S. Weil, J. Solid State Chem. 181 (1) (2008) 199–210.
[39] D.G. Nam, N. Kang, Y.S. Kim, H.C. Lee, Met. Mater. Int. 15 (2) (2009) 273–278.
[40] K.H. Lee, S.H. Lee, J.H. Kim, Y.Y. Lee, Y.H. Kim, M.C. Kim, D.M. Wee, Int. J. Hydrogen Energy 34 (3) (2009) 1515–1521.
[41] T.J. Toops, M.P. Brady, P.F. Tortorelli, F. Estevez, D. Connors, F. Garzon, T. Rockward, J. Pihl, D. Gervasio, W. Mylan, H. Kosaruju, J. Power Sources 195 (2010) 5619–5627.
[42] M.P. Brady, et al., 2008 Annual Report, United States Department of Energy Hydrogen, Fuel Cells, and Infrastructure Program, report V.B.1 (2008) 844–848. http://www.hydrogen.energy.gov/pdfs/progress08/v_b_1_brady.pdf.
[43] I. Paulauskas, M.P. Brady, H.M. Meyer III, R.A. Buchanan, L.R. Walker, Corros. Sci. 48 (10) (2006) 3157–3171.